Available online at www.sciencedirect.com
SCIENCE DIRECT®
Electrochimica Acta 49 (2004) 1127–1140
ELECTROCHIMICA Acta
www.elsevier.com/locate/electacta

Influence of substrate microstructure on the growth of anodic oxide layers

L.E. Fratila-Apachitei [a,*], H. Terryn [b], P. Skeldon [c], G.E. Thompson [c], J. Duszczyk [a], L. Katgerman [a]

[a] *Department of Materials Science & Technology, Delft University of Technology (TUD), Rotterdamseweg 137, 2628 AL Delft, The Netherlands*
[b] *Department of Metallurgy, Vrije Universiteit Brussel, Electrochemistry and Materials Science, Pleinlaan 2, 1050 Brussel, Belgium*
[c] *Institute of Science and Technology, Corrosion and Protection Centre, University of Manchester P.O. Box 88, Manchester M60 1QD, UK*

Received 31 July 2003; received in revised form 17 October 2003; accepted 26 October 2003

Abstract

The effects of permanent mold cast microstructure on the growth of anodic oxide layers on three different aluminum substrates (i.e. Al99.8, AlSi10, and AlSi10Cu3, wt.%) were investigated by optical microscopy (OM), scanning electron microscopy (SEM), and laser scanning confocal microscopy (LSCM). The anodic oxidation was performed galvanostatically in 2.25 M H_2SO_4, at 0 °C. The oxide layers developed a microscale topography mainly determined by the morphology of aluminum grains and cells. A low amount of insoluble impurities, uniformly distributed, would contribute to the growth of oxide layers with minimum defects and uniform thickness on the pure aluminum substrate whereas for the binary and ternary systems, a fine cell structure and a modified morphology of Si particles would be favorable. The Al–Fe and Al–Fe–Si particles were occluded in the oxide layers next to Si particles, blocking locally the oxide growth whereas Al_2Cu particles were preferentially oxidized. In addition, the presence of Si particles in the layer influenced pore morphology by development of deflected pores around the particles.

Keywords: Anodic oxidation; Microstructure; Anodic oxide layers; Morphology; Second phase particles

1. Introduction

Anodic oxidation of aluminum continues to find applications in areas such as, membrane technology and microelectronics for production of ordered nanoscale structures [1–10], as a cost-effective and readily to implement process. In these fields, the research is focused mainly on tailoring the process for a desired pore and cell morphology. In the case of aluminum alloys, however, the process still encounters problems related to the growth of sufficiently thick or hard layers (i.e. hard anodizing process), particularly on highly alloyed substrates, such as 2*xxx* (Al–Cu–Mg), 7*xxx* (Al–Zn–Mg) wrought and 3*xx.x* (Al–Si–Cu), and 4*xx.x* (Al–Si) cast alloys [11–14]. The reasons are believed to be related to the presence of second phase particles that affects surface reactivity during pretreatment and during anodic oxidation, assisting secondary reactions that determine local changes in surface/oxide composition and morphology [15–19]. Therefore, efforts are increasingly directed on understanding the relations between alloys microstructure and anodic behavior, as a necessary step in closing the substrate–(anodic oxidation) process–coating knowledge chain, rather than looking only at the process per se or resultant coating properties.

This trend is also observed for other types of surface treatments (e.g. chemical and electrochemical polishing) and also in corrosion research, being enabled and supported by the availability of the advanced microscopy and electrochemical measurement techniques, like atomic force microscopy (AFM), laser scanning confocal microscopy (LSCM), scanning Kelvin probe microscopy (SKPM), scanning vibrating electrode techniques (SVET), medium-energy ion scattering (MEIS) [19–22]. One of the outputs of these studies is the major role of impurities with high melting point or low solid solubility in aluminum, that segregate at cellular boundaries during casting and determine the development of specific local nanotextures following surface treatments [23,24]. Therefore, this research opens the possibility of un-

* Corresponding author. Tel.: +31-15-2789083; fax: +31-15-2786730.
E-mail address: e.l.apachitei@tnw.tudelft.nl (L.E. Fratila-Apachitei).

0013-4686/$ – see front matter © 2003 Elsevier Ltd. All rights reserved.
doi:10.1016/j.electacta.2003.10.024

derstanding local processes that eventually determine the properties of a certain coating/surface, and also the engineering of surfaces at the micron and nano-scales by controlling their microstructure and composition.

Low solid solubility impurities, e.g. iron and silicon, are encountered in commercially pure aluminum alloys. In cast compositions, silicon and copper are present at relatively large concentrations, that exceed their solid solubility in alloy, and therefore mainly in the form of coarse intermetallic particles. Anodic oxidation of these alloys usually results in formation of thin, soft, and powdery layers, with a high propensity for "burning" (i.e. local dissolution of the layer and underlying alloy) [25]. The co-existence of more than two second phases in the same aluminum matrix (i.e. ternary systems or more) having different anodic behavior poses challenges to the fundamental understanding of anodizing processes.

Much of the available literature refers to dilute, binary, model aluminum alloys with alloying elements retained largely in the solid solution, and to conventional anodizing process (i.e. room temperature, $<2.0\,A\,dm^{-2}$ and few minutes oxidation to barrier or porous layers). Relatively very few data are available on highly alloyed cast aluminum substrates or hard anodizing conditions [26–30], despite the applications in the automotive, aircraft, and other industries. At present, the hard anodizing process is difficult to control and the scrap rates are high due to the unpredictability of the response of various cast compositions and microstructures.

The morphological changes induced by substrate microstructure during the growth of thick and porous anodic oxide layers on three different aluminum alloys (i.e. Al—99.8 wt.%, Al—10 wt.%Si, and Al—10 wt.%, Si—3.2 wt.% Cu) are investigated in this study by optical microscopy (OM), laser scanning confocal microscopy and scanning electron microscopy combined with energy dispersive X-ray spectroscopy (SEM/EDS). Both the anodic oxidation conditions and substrate compositions were selected to be relevant to the industrial practice.

2. Experimental

2.1. Aluminum substrates

The aluminum substrates were produced by permanent mold casting as described previously [19]. The cast bars were cut and machined to form disk-shaped specimens of 45 mm diameter and 7.0 mm thickness. Their chemical composition, as determined by X-ray fluorescence (XRF), is included in Table 1.

2.2. Anodic oxidation

Prior to anodizing, the samples were ground and polished using a Struers RotoPol 31 automated system (220-grade SiC paper 1.5 min; 9 μm diamond suspension, 10 min; 6 μm, and 3 μm diamond suspension, 5 min each; colloidal silica, 1 min). Ultrasonic cleaning of the samples and the holder, in ethanol for about 30 s, was performed between the successive polishing steps. Finally, the samples were ultrasonically cleaned in isopropanol for 15 min. Unless otherwise specified, anodic oxidation was performed at a current density of $4.2\,A\,dm^{-2}$ in 2.25 M H_2SO_4 at 0 °C for 50 min. After anodizing, the specimens were rinsed in demineralized water for about 3 min, oven dried (50 °C, 30 min), and stored in a desiccator.

2.3. Macroscopic examination of the aluminum substrates

Surface macro-examination of the substrates was performed after macro-etching with Poulton's reagent (12 ml HCl, 6 ml HNO_3, 1 ml HF, 1 ml H_2O) to reveal grain morphology.

2.4. Microscopic examination by optical microscopy

The surface microstructure of the substrates prior to anodizing and the morphology of oxide cross-sections were assessed by optical microscopy. For the former purpose, the samples were polished as previously stated whereas for the latter, the specimens were firstly cut and mounted in resin and thereafter polished using a similar program, except that for each step shorter times were used [19]. No etching was necessary to reveal the second phases. Next to the morphology of the entire section of the oxide layers, the optical microscopy was used to measure oxide layer thickness along the specimens' diameter. The results represent the average and standard deviations of approximately 70 readings for each specimen. The standard deviation indicated oxide thickness uniformity along the specimen diameter.

Table 1
Chemical composition (wt.%) of the aluminum substrates

Substrate	Al	Si	Cu	Ti	Fe	Mg	Mn	Zn, Ni, Cr, Sn, Pb
Al	99.80	0.03	<0.01	<0.01	0.08	<0.01	<0.01	<0.02
AlSi10[a]	89.70	9.97	0.01	0.02	0.21	0.03	<0.01	<0.02
AlSi10Cu3[a]	85.95	10.50	3.22	0.02	0.21	<0.01	<0.01	<0.02

[a] Sr–0.015 wt.%

2.5. Scanning electron microscopy and energy dispersive spectroscopy

The chemical composition and the morphology of second phase particles were further investigated by SEM/EDS (microscope JEOL JXA 8900R equipped with a combined wavelength and energy dispersive, WD/ED microanalyser) using an electron beam energy of 15 keV and a beam current of 40 nA. The X-ray spectra were recorded using a Noran Pioneer Energy Dispersive Spectrometer. Polished cross-sections of the anodized specimens, coated with a thin layer of carbon were prepared, thus enabling the examination of the substrate, substrate/oxide interface and oxide layer per se in relation to the behavior of second phase particles. Elemental mapping of the substrate/oxide interface for Si, Fe, and Cu was performed using a beam current of 99 nA. In addition, oxide fracture sections, produced under liquid nitrogen (i.e. cryofractures) were coated with a gold layer of approximately 1 nm and examined by SEM (JEOL JSM 840A) to reveal preliminary information on the morphology of the pores for the different anodic oxide layers. In this case, an accelerating voltage of 15 kV was used.

2.6. Topography of the anodic oxide layers

The morphology of the surface of the oxide layers was examined by LSCM using a Leica TCS SP multiband confocal imaging spectrophotometer interfaced with a computer equipped with the Leica software [19]. 3D topographical images from different grain zones were obtained by data post-processing.

2.7. Surface roughness of the anodic oxide layers

A surface profilometer type Surtronic 3+ was used to measure surface roughness R_a of the anodic oxides. At least six readings were performed for each grain zone using a cut-off length of 0.8 mm and an evaluation length of 8 mm.

3. Results and discussion

The use of disk-shaped specimens, comprising cross-sections of the cast bars, enabled investigation of the effects of substrate microstructure, including structural changes occurring across specimen thickness during solidification, on the morphology of the anodic oxide layers. The latter may help in understanding the implications of different casting processes or parameters on the anodic behavior of the resultant cast microstructure. For each composition, the effects of aluminum grains and cells morphology are firstly presented, followed by the effects of second phase particles. To be mentioned that cells are contained by grains. For clarity, the term grain was used in the case of pure aluminum substrate. For the binary and ternary compositions, the distinction is much clear due to the presence of silicon phase and therefore, the appropriate terms were used.

3.1. Influence of aluminum grain and cell morphology on oxide growth

Two different grain morphologies were revealed by macro-etching of the aluminum substrate, i.e. columnar grains at the outer zone and coarse equiaxed grains towards the center (Fig. 1a). Most probably, the zone of fine equiaxed grains usually present close to the surface, as a result of high nucleation and solidification rates, has been lost due to machining following casting, when up to 2.5 mm of surface material was removed.

With silicon added to the melt, the microstructure changed significantly (Fig. 1b). The grains were of reduced size, with

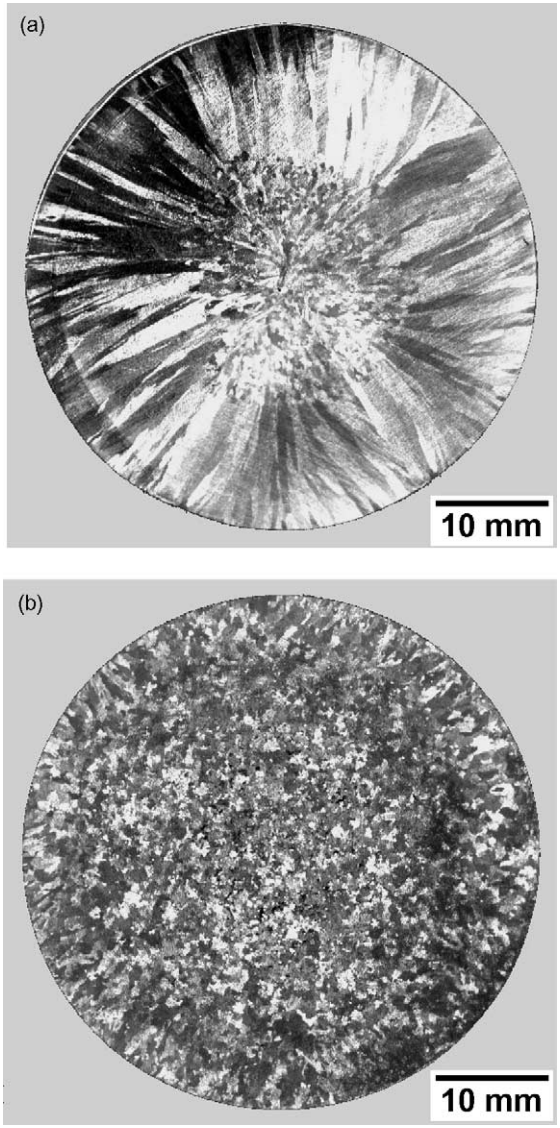

Fig. 1. Grain morphology of the (a) Al and (b) AlSi10 substrates as revealed by macro-etching using Poulton's reagent.

a very narrow columnar zone compared with the pure aluminum substrate. For this substrate, part of the zone of fine equiaxed grains at the outer area was still present. The finer grain structure compared with pure aluminum is determined by silicon acting as a grain refiner [31,32]. In addition, pores originating from the casting process (black spots) are visible, mainly in the center. The ternary composition had, in general, a similar grain structure to the binary substrate.

The disk-shaped substrates underwent anodizing in 2.25 M H_2SO_4 maintained at 0 °C for 50 min, using 3.0, 4.2, and 6.0 A dm^{-2}. Distribution of oxide layer thickness along specimens diameter as well as its uniformity (i.e. standard deviation) are presented in Fig. 2. The results indicate the development of an oxide layer of uniform thickness regardless of the grain morphology and current density for aluminum, whereas the binary and ternary compositions revealed an increased non-uniformity in the center, i.e. the area corresponding to the coarse equiaxed grains.

The topography of the anodic oxide layer grown on the aluminum substrate is shown in Fig. 3. Similar micrographs for the non-anodized substrates revealed a relatively smooth surface [19]. Increased roughness observed locally in Fig. 3 could be generated by the presence of insoluble impurities having a different anodic response relative to the matrix or by oxide surface cracks.

Previous investigations of the early stages of pores formation during anodic oxidation in H_2SO_4 at room temperature [33–35] indicated preferential pore development at grain boundaries, and scratches or specific surface texture resulted for example from cold working, were still present. The effect was called pore alignment or epitaxial growth, although the latter refers rather to the continuation of surface crystallographic structural features into the oxide film [36].

The topography and cross-section morphology of the oxide layers above the fine and coarse equiaxed regions for the AlSi10 substrate are shown in Figs. 4 and 5, respectively.

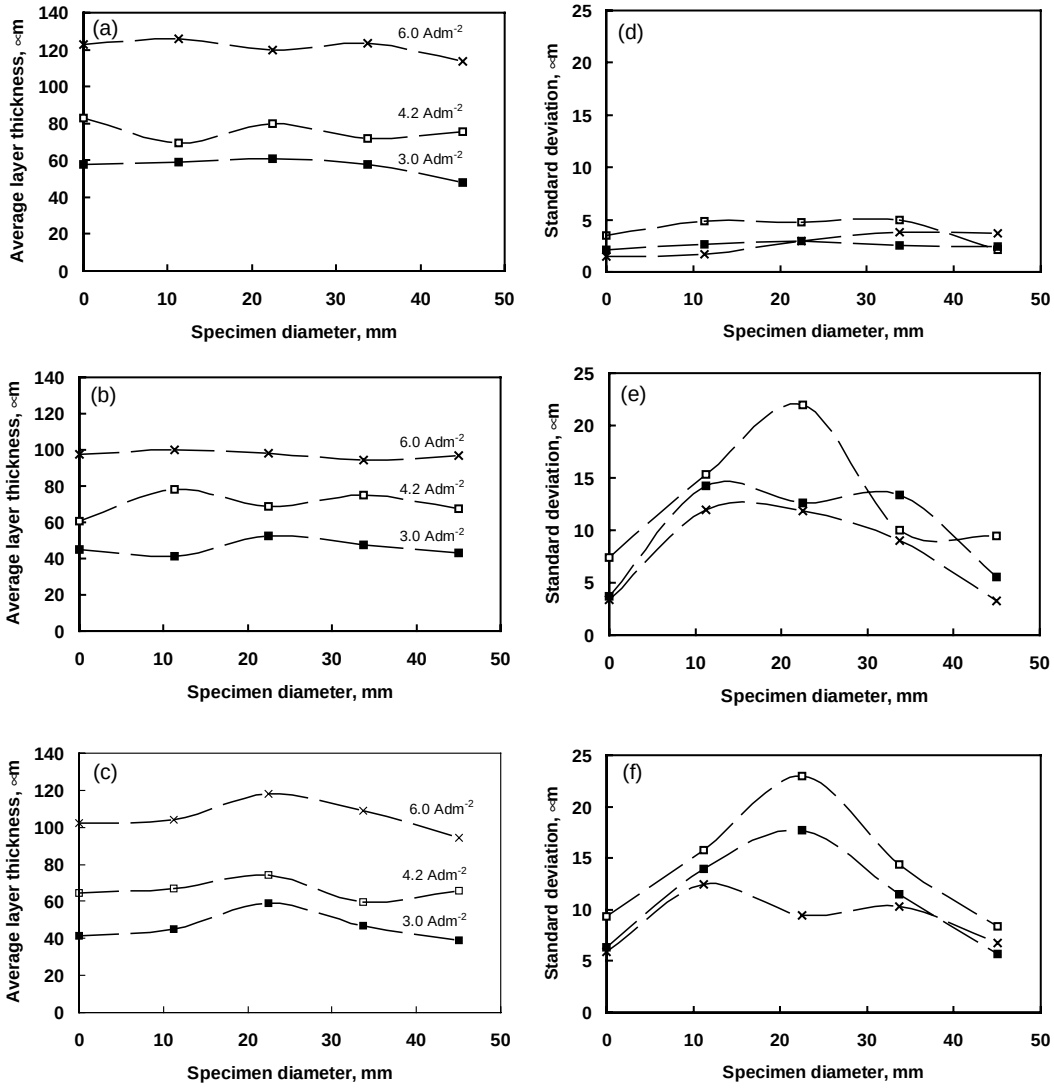

Fig. 2. Distribution of oxide layer thickness along the specimen diameter for anodic oxides formed on: (a, d) Al, (b, e) AlSi10 and (c, f) $AlSi10Cu_3$ substrates at 3.0, 4.2, and 6.0 A dm^{-2} (2.25 M H_2SO_4, 50 min, 0 °C).

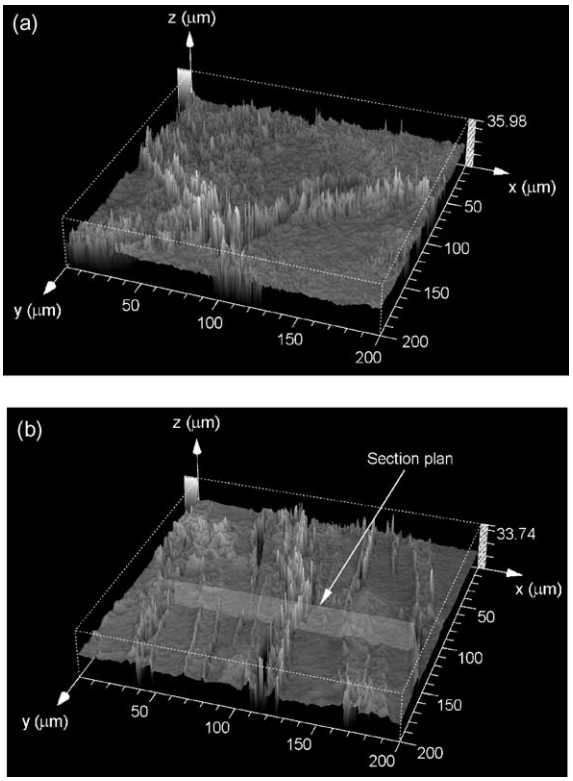

Fig. 3. Topography of the anodic oxide layer formed on the aluminum substrate over the (a) equiaxed and (b) columnar grains (2.25 M H_2SO_4, 3.0 A dm^{-2}, 50 min, 0 °C). 3D LSCMs.

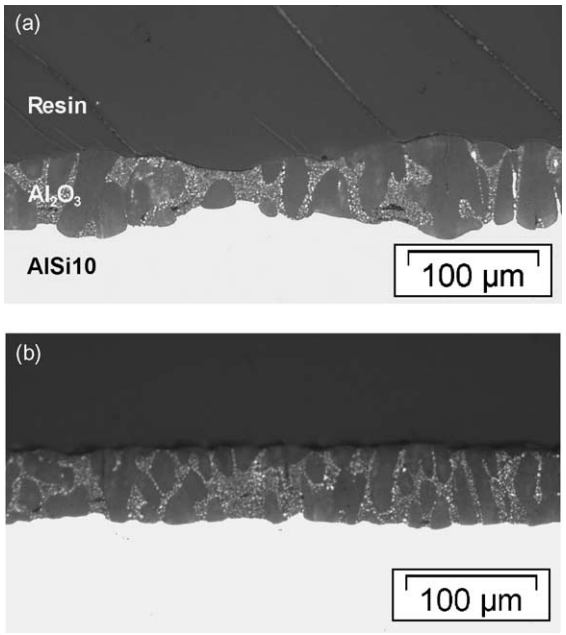

Fig. 5. Optical micrographs of the oxide cross-sections formed on the AlSi10 substrate in the: (a) coarse and (b) fine grain zones (2.25 M H_2SO_4, 3.0 A dm^{-2}, 50 min, 0 °C).

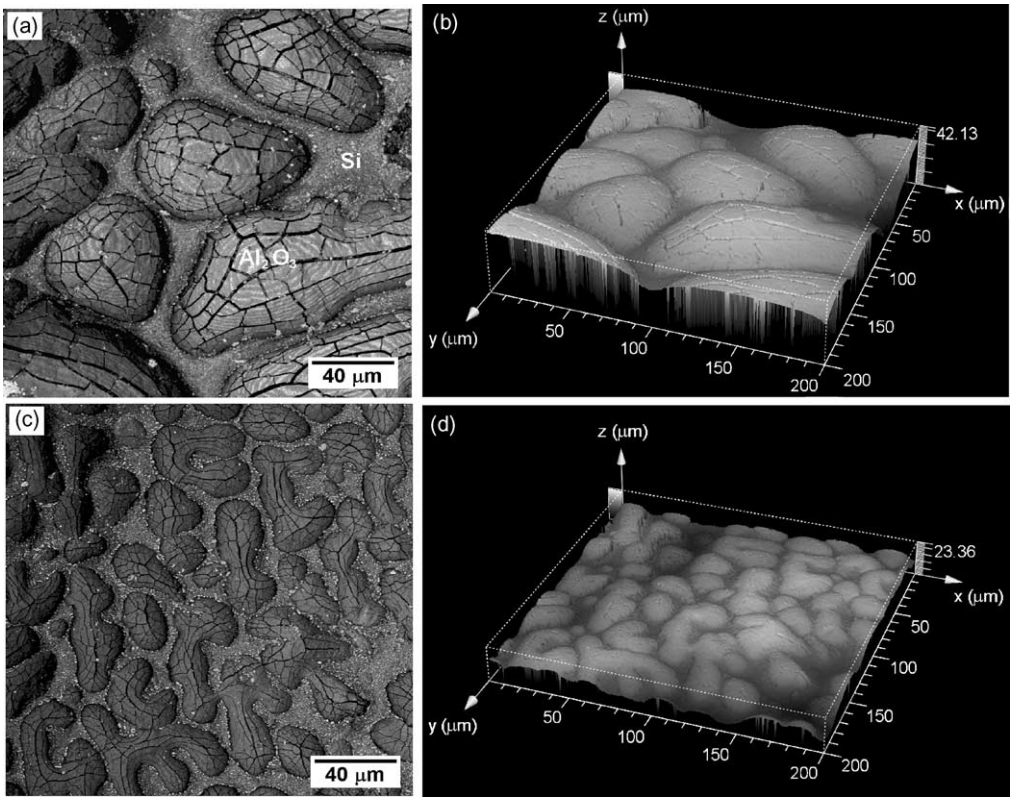

Fig. 4. Oxide layer topography for the AlSi10 substrate corresponding to coarse grains: (a) 2D LSCM, (b) 3D LSCM and fine grains: (c) 2D LSCM, (d) 3D LSCM (2.25 M H_2SO_4, 3.0 A dm^{-2}, 50 min, 0 °C).

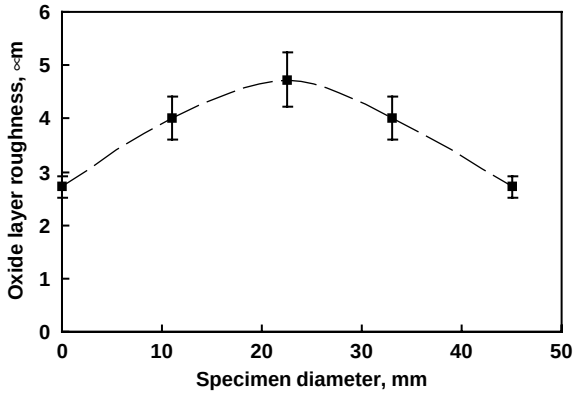

Fig. 6. Distribution of oxide layer surface roughness along the specimen diameter for anodic oxides formed on AlSi10 substrate at 3.0 A dm^{-2} (2.25 M H_2SO_4, 50 min, 0 °C).

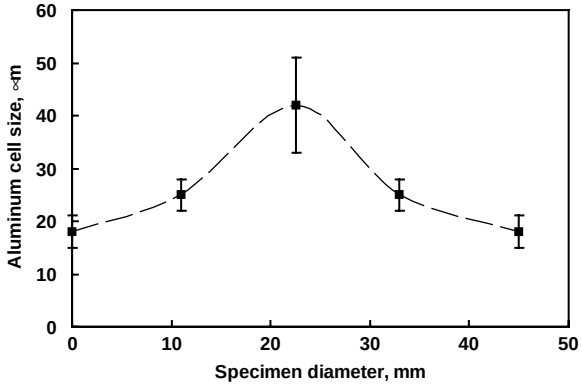

Fig. 8. Variation of aluminum cell size along the diameter of the AlSi10 specimen.

The oxide layer seems to preserve the microstructure of the substrate. A coarser oxide topography is associated with the region of large grains (Fig. 4a and b) compared with the finer topography at the outer zones corresponding to the fine aluminum grains (Fig. 4c and d). Because of the presence of (α-Al + Si) eutectic, the substrate/oxide and oxide/electrolyte interfaces became scalloped (Fig. 5) with a more pronounced effect in the middle, i.e. region of the large grains. In addition, oxide surface roughness indicated the same trend i.e., largest values at the center of the specimens (Fig. 6).

A scrutiny of the microstructure of the AlSi10 substrate by optical microscopy (Fig. 7) revealed aluminum cells of

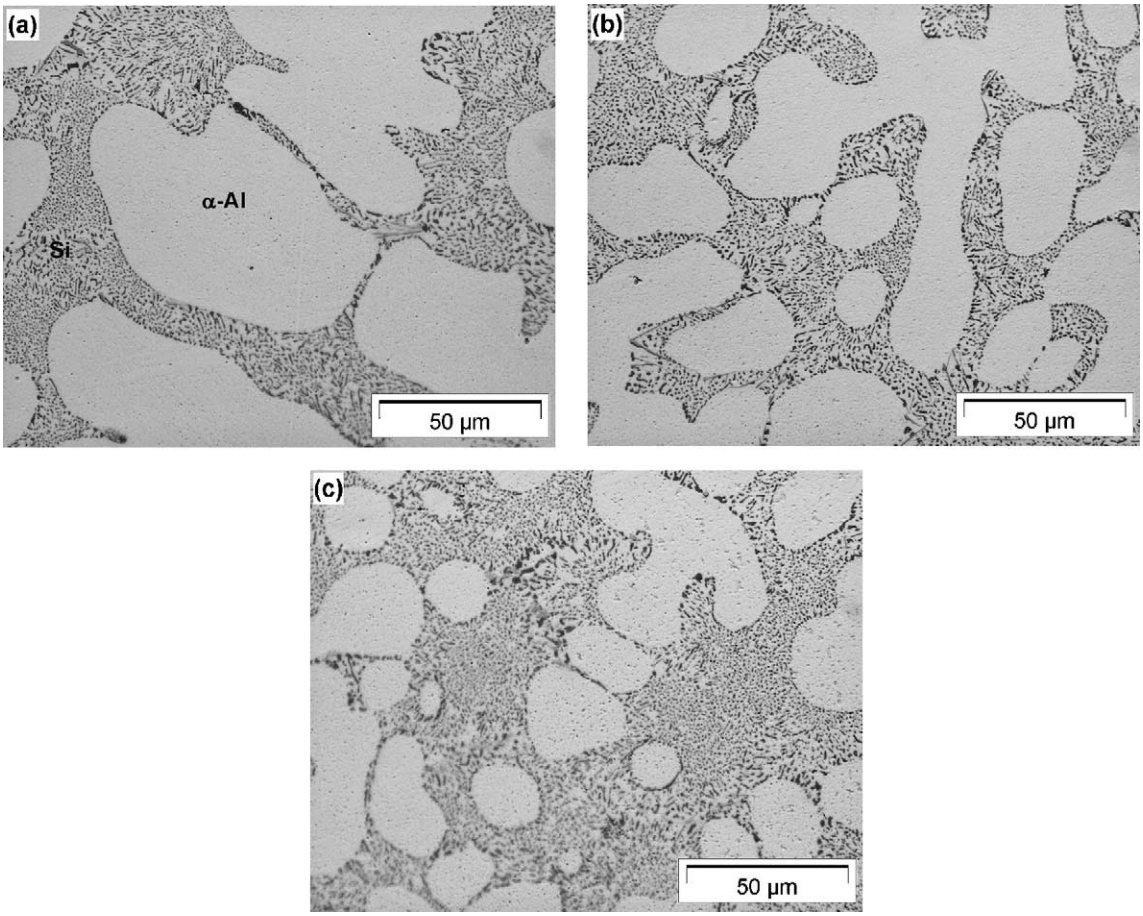

Fig. 7. Optical micrographs for the AlSi10 substrate showing distribution of Si particles and morphology of aluminum cells in the (a) coarse, (b) columnar and (c) fine grain zones.

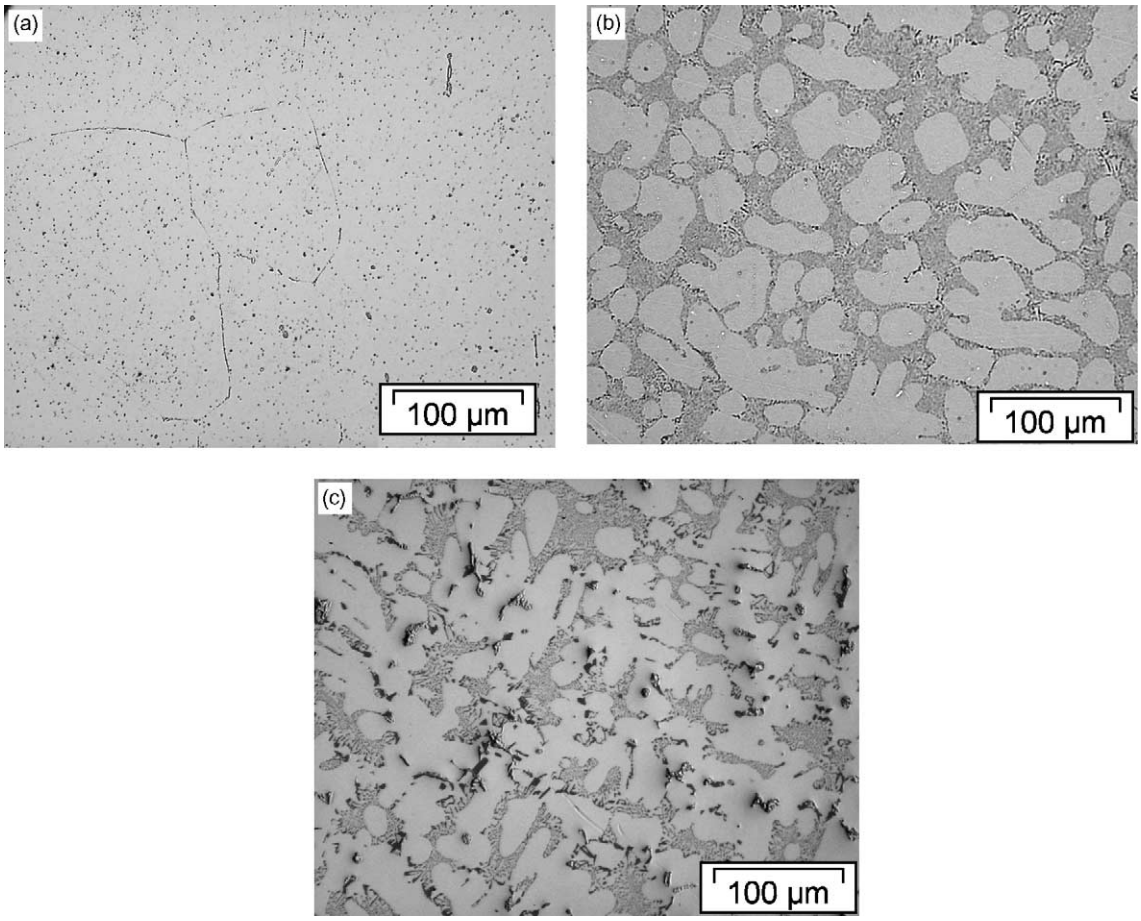

Fig. 9. Distribution of second phase particles as revealed by optical microscopy for (a) Al; (b) AlSi10; (c) AlSi10Cu3 substrates.

different morphology corresponding to the three different grain zones (i.e. fine, columnar, and coarse). The variation of cell size along the diameter of the specimens is shown in Fig. 8. The results indicate that a fine microstructure, ensured by small and uniform cells, may be the first necessary condition to improve the uniformity of the overlying oxide layer, as the reactivity of the surface becomes more uniform. The same behavior is shown by the ternary substrate since silicon is the dominant alloying element that determines the microstructure.

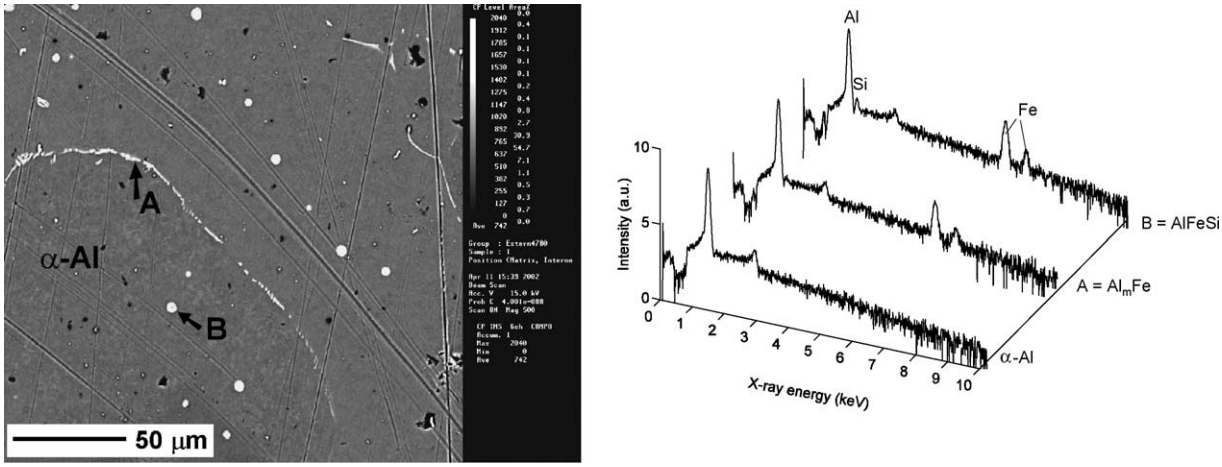

Fig. 10. SEM micrograph and EDS spectra of the second phases observed for the aluminum substrate.

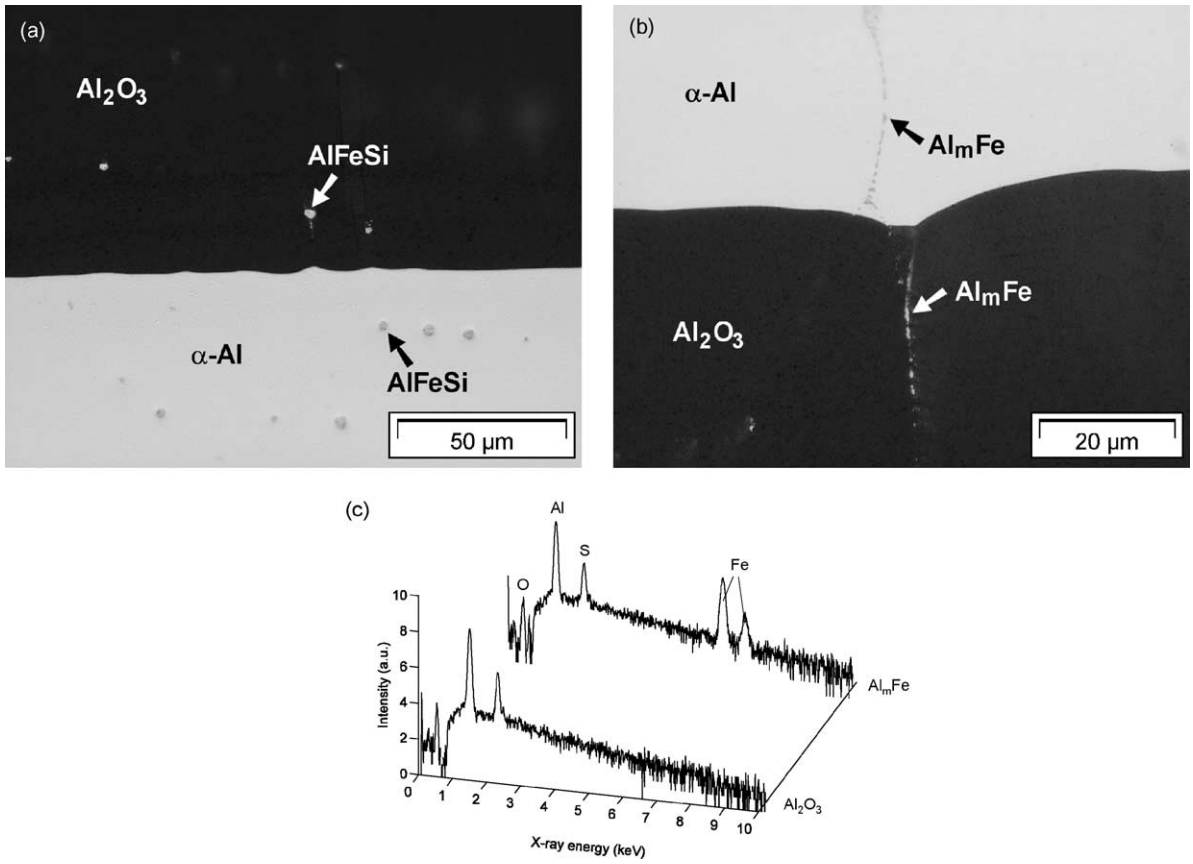

Fig. 11. The effects of iron bearing particles on the growth of anodic oxide layers on aluminum substrate: (a) AlFeSi; (b) Al_mFe; (c) EDS spectra of the oxide matrix and an Al_mFe particle occluded in the layer (Al, 2.25 M H_2SO_4, 4.2 A dm^{-2}, 50 min, 0 °C).

3.2. Influence of second phase particles on oxide growth

The typical microstructure of the three aluminum substrates showing the distribution and morphology of second phases is represented in Fig. 9.

3.2.1. Aluminum substrate

The aluminum substrate contained 0.03 wt.% Si, and 0.08 wt.% Fe impurities, as determined by XRF (Table 1). Their maximum solid solubility in binary aluminum alloys is 1.65 and 0.05 wt.%, respectively [37]. However, in

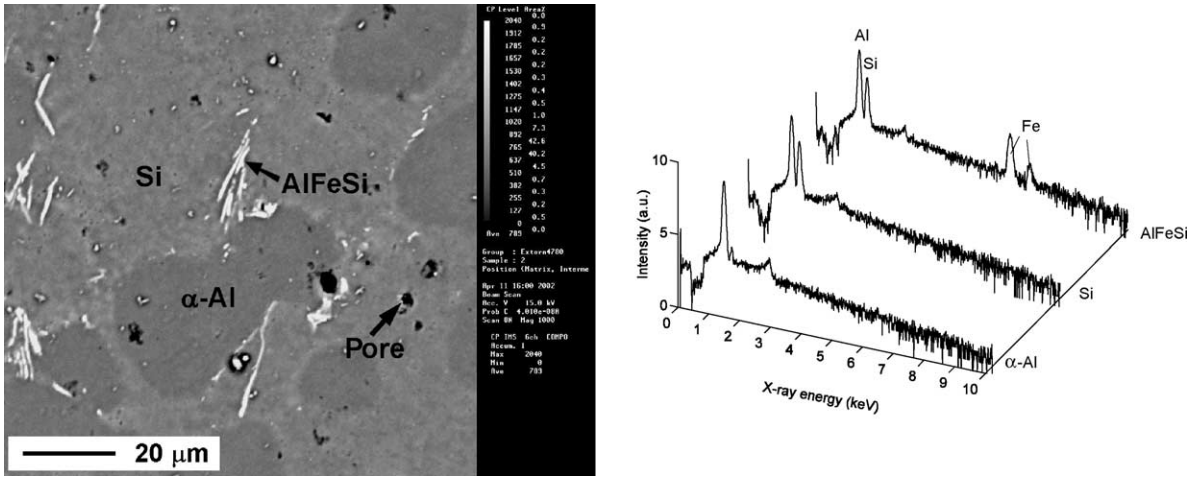

Fig. 12. SEM micrograph and EDS spectra of the second phases observed for the AlSi10 substrate (Si particles are not readily visible due to the proximity of the characteristic lines of Al and Si).

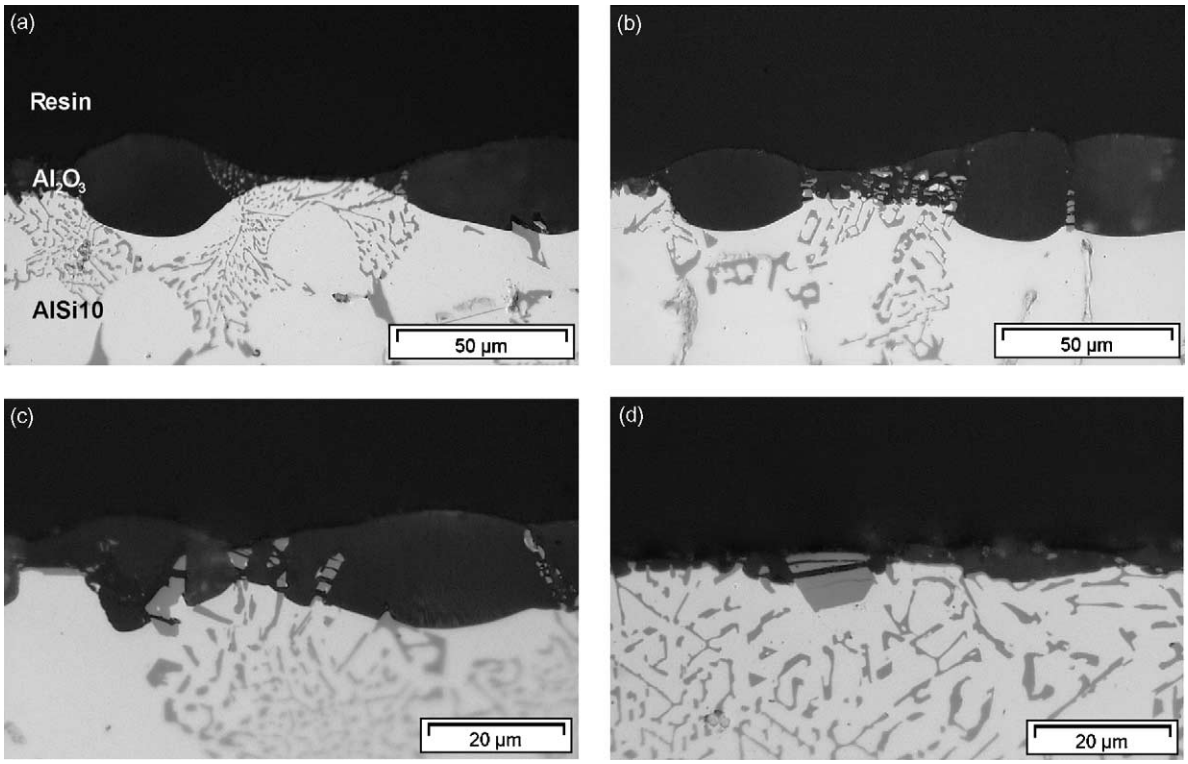

Fig. 13. Influence of Si particles on the growth of anodic oxide layers (2.25 M H_2SO_4, 4.2 A dm^{-2}, 10 min, 0 °C).

the presence of additional impurities or alloying elements and at room temperature, their solubility decreases significantly (e.g. about 0.05 at.% for silicon at 300 °C [38] and ≤0.01 wt.% for iron in the presence of additional impurities [39]). Thus, iron forms second phase particles during solidification, usually phases of Al–Fe or Al–Fe–Si type [39]. Previous analysis by XRD [19] could not identify iron bearing second phases although they were observed by optical microscopy, mainly at grain boundaries (Fig. 9a). Further SEM/EDS analyses revealed the spectra included in Fig. 10, where the presence of iron bearing intermetallics is evident. In addition, gas porosity originated from casting are observed as black spots (2–9 μm diameter) in the microstructure.

The cooling rates during the casting process were estimated between 1 and 20 °C s^{-1} from the cell size of the binary AlSi10 substrate. At these rather high rates, the formation of metastable phases such as Al_mFe and Al–Fe–Si

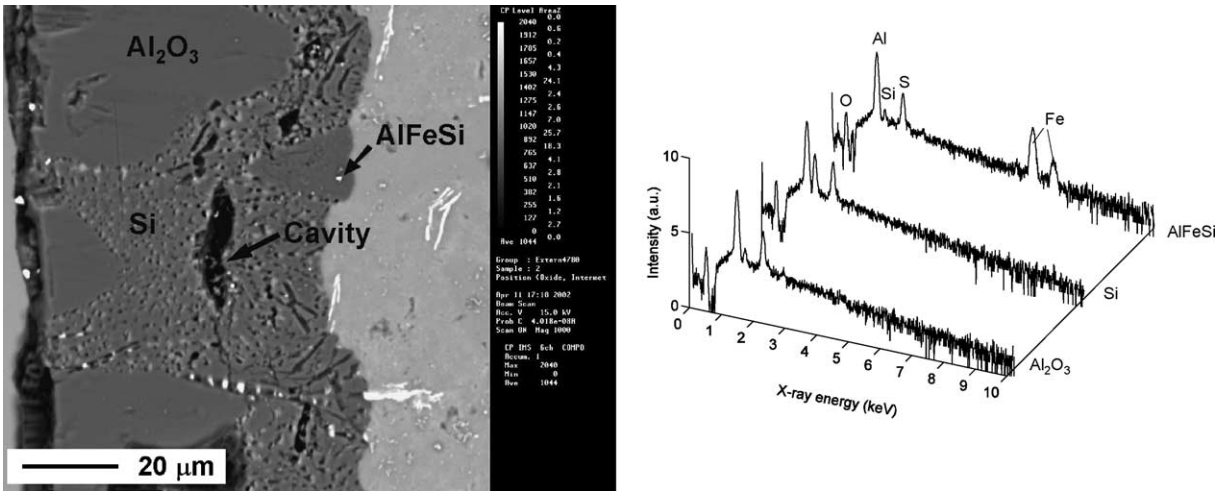

Fig. 14. SEM micrograph and EDS spectra of the anodic oxide layer formed on the AlSi10 substrate (2.25 M H_2SO_4, 4.2 A dm^{-2}, 50 min, 0 °C).

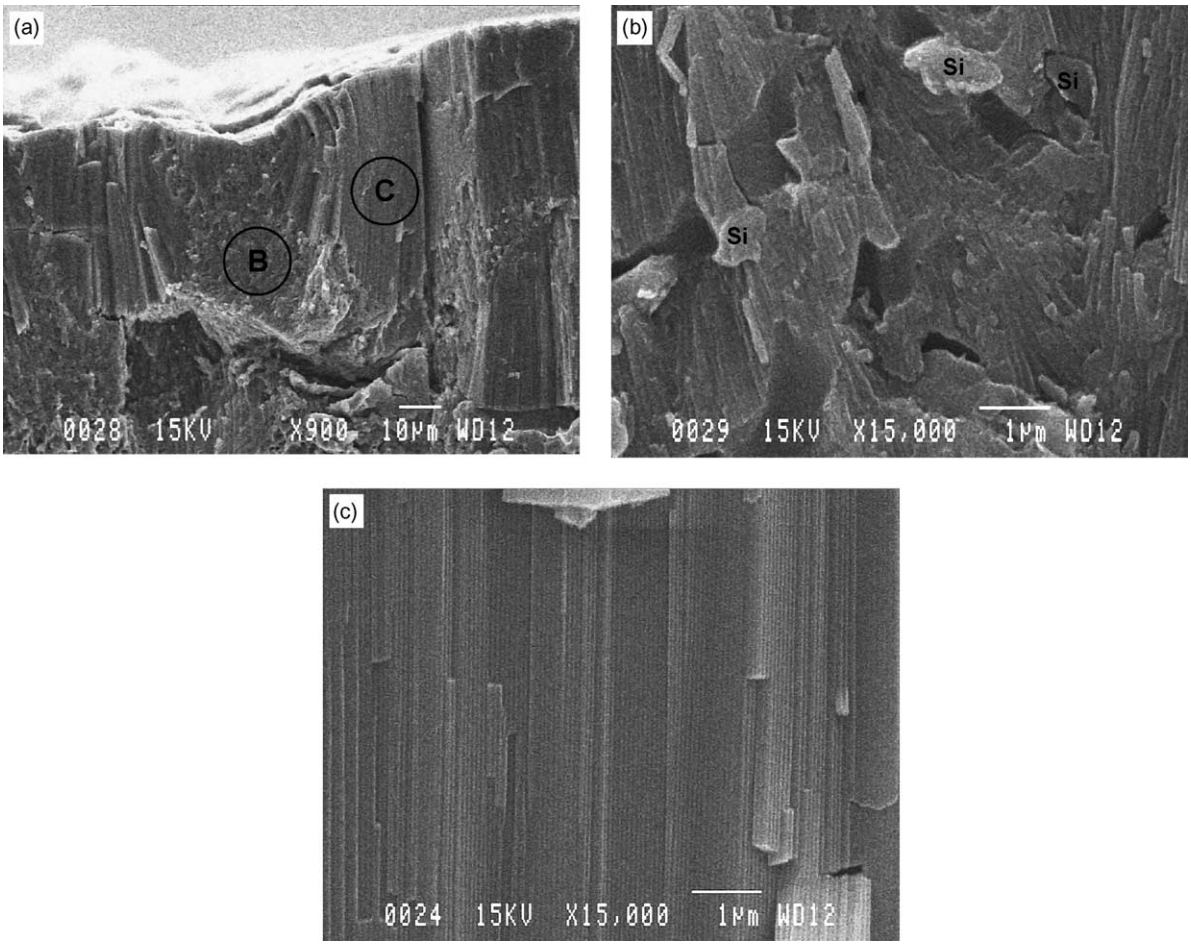

Fig. 15. Effects of Si particles on the oxide pore morphology as revealed by SEM analysis of cryofractures: (a) an overview of the entire oxide cross-section; (b) enlarged image of silicon rich zone B; (c) enlarged image of zone C, free of silicon (AlSi10, 2.25 M H_2SO_4, 4.2 A dm^{-2}, 50 min, 0 °C).

is favored relative to the equilibrium Al_3Fe phase (usually encountered in commercially pure aluminum alloys), that forms at cooling rates less than 1 °C s^{-1} [40]. According to (i) the EDS results, (ii) the composition of aluminum substrate (i.e. a Fe/Si ratio of 2.6) and (iii) the cooling rates during casting, particles A (more numerous and mainly present along the grain boundaries) were identified as Al_mFe whereas particles B (rounded, 2–5 μm size, located inside

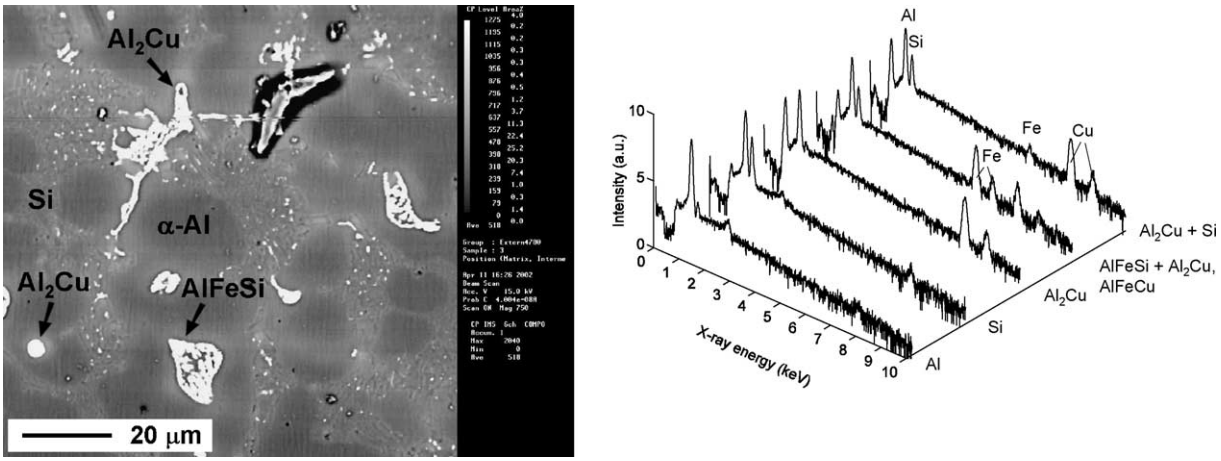

Fig. 16. SEM micrograph and EDS spectra of the second phases observed for the AlSi10Cu3 substrate.

the grains) as α-AlFeSi (Fig. 10). Due to the variation of the cooling rates from the mold wall towards the center of the cast bars, gradients in phase composition may appear with preferential formation of Al_mFe at higher cooling rates (i.e. at the outer areas of the specimens) whereas Al_6Fe and new Al_xFe phases are likely to form at lower cooling rates (i.e. towards the center) [40,41].

The effects of these particles on the morphology of anodic oxide layers are shown in Fig. 11. Both types of particles were occluded in the oxide layer and, as a consequence, the substrate/oxide interface became locally scalloped. These findings indicate that the iron bearing particles present in the aluminum substrate are either inert or undergo oxidation at a lower rate compared with the adjacent aluminum matrix. Previous studies [42] on Al—0.5 wt.% Fe and Al—1.4 wt.% Fe alloys anodized in H_2SO_4 at 25 °C revealed that Al_6Fe particles were partially oxidized and partially incorporated in the oxide layer whereas the Al_3Fe particles oxidized at the same rate with the aluminum matrix and thus could not be entrapped in the layer. Therefore, the absence of Al_3Fe particles in the aluminum substrate is further supported by the anodizing behavior observed for the iron bearing particles.

The above findings indicate that the quality of anodic oxide layers formed on the pure aluminum substrate under the specified conditions will depend on the amount and distribution of insoluble impurities that have a different behavior relative to the matrix during anodizing. Therefore, increasing aluminum purity and ensuring an uniform distribution of the impurities, possibly by an uniform grain morphology, would generate a suitable microstructure for this substrate in the view of anodizing.

3.2.2. AlSi10 substrate

Next to the iron containing particles (i.e. blades of AlFeSi), Si particles present in an eutectic structure dominate the microstructure of the binary system (Figs. 9b and 12), reducing the volume fraction of α-Al available for oxidation. Silicon particles were modified using strontium. As a result, fine particles (<5 μm) were mainly formed during solidification. Occasionally larger, partially modified particles (5–20 μm) are observed in the form of flakes or needles. The influence of Si particles morphology on the growth of oxide layers is illustrated in Fig. 13 that depicts the substrate/oxide interface for oxide layers formed at 4.2 A dm^{-2} and short anodizing duration (i.e. 10 min).

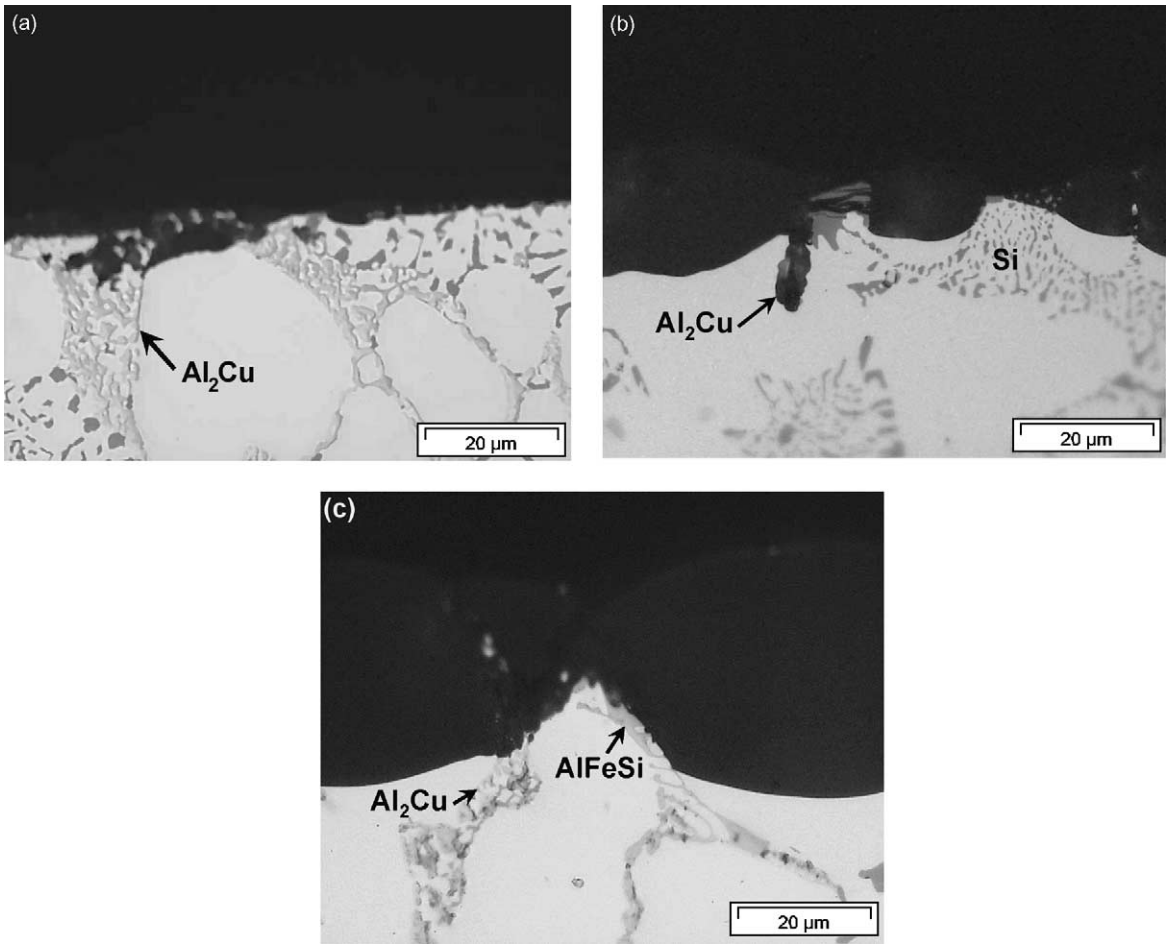

Fig. 17. The effect of second phases on the growth of anodic oxide layer on the AlSi10Cu3 substrate (2.25 M H_2SO_4, 4.2 A dm^{-2}, 10 min, 0 °C).

When the oxide front encounters a well-modified Si particle, current distribution changes in favor of less resistive adjacent aluminum matrix. As a consequence, the oxide grows around the particle until it is completely entrapped in the layer, apparently causing no defects. The effect is a non-uniform thickness of the oxide that was observed for the entire corresponding eutectic structure, relative to the α-Al solid solution (Fig. 13a and b). When a partially modified Si particle is approached, the oxide front attempts to penetrate the particle (Fig. 13c and d). In general, when such larger particles are present, their entrapment disturbs more significantly the uniform growth of the oxide determining large variation in oxide thickness locally, cracks formation and increased roughness at the interface substrate/oxide. The resultant oxide layer resembles a composite material, with the aluminum oxide representing the matrix and Si particles the occluded particles (Figs. 5 and 14). The iron containing particles were also detected in the oxide layer (Fig. 14).

Based on the findings for the AlSi10 substrate, fine cell structures and modified Si particles seem to result in a suitable microstructure for growing relatively uniform oxide layers with less defects associated with Si particles. In the case of the permanent mold cast process, efficient modifiers and high cooling rates (or thin mold walls) should be used. Higher cooling rates are also achieved by die casting processes.

Under specific anodizing conditions (e.g. extended anodizing times under high current densities) defects in the form of cavities, associated with oxidation of the eutectic structures could be observed in the layer (Fig. 14). A preliminary indication of the effects of occluded Si particles on oxide pore morphology is illustrated in the SEM cryofractures (Fig. 15). The tortuous porosity (mainly branching and deflection of the pores) developed around Si particles is clearly observed. It is expected that, in addition to the size and shape of Si particles, the distance between particles in an eutectic structure will also influence the quality of the oxide layers, due to possible overlapping of particles' zone of influence (i.e. the oxide area affected around the particles).

3.2.3. AlSi10Cu3 substrate

When copper was added to the binary system in the specified concentration, a new intermetallic phase was formed during solidification, namely the Al_2Cu present as large, globular or irregular particles (3–20 μm) mostly near to Si particles (Fig. 16).

The effects of second phase particles in the ternary substrate on the growth of oxide layers are illustrated in Fig. 17 that includes the optical micrographs of the substrate/oxide interface of oxide layers grown at 4.2 A dm^{-2} for 10 min. Whenever Al_2Cu is present at the substrate/oxide interface, the oxide front advances more rapidly towards the particle as current distribution changes in favor of the less resistive particle (Fig. 17a and b). The competition ends when the particle is completely oxidized and the current distribution changes again in the favor of the residual aluminum around until a new copper containing particle is encountered. Thus, the layer growth becomes non-uniform. In addition, large voids are left behind due to particle oxidation and

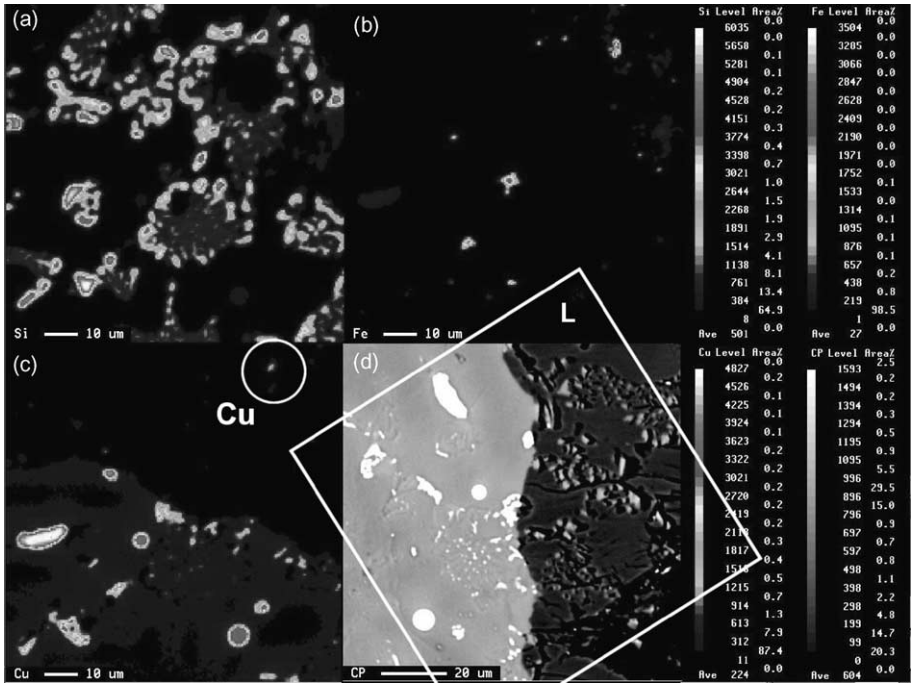

Fig. 18. Elemental maps for (a) Si; (b) Fe; and (c) Cu together with the SEM micrograph; (d) for the interface substrate/oxide (AlSi10Cu3, 2.25 M H_2SO_4, 4.2 A dm^{-2}, 50 min, 0 °C). L indicates the upper left corner in (a), (b), and (c).

dissolution, increasing the porosity of the oxide with consequences on properties like Vickers microhardness [43].

When Al_2Cu, Si, and AlFeSi adjacent particles are present at the substrate/oxide interface (Fig. 17b and c), the disturbance is more pronounced as the front advances fastest towards the copper intermetallic, then to the surrounding aluminum whereas Si and AlFeSi particles block the growth of the oxide. As a result, the layer presents a large variation in thickness at these regions. The interface ternary substrate/oxide becomes very dynamic with continuous changes in current distribution between aluminum matrix, silicon, iron, and copper containing particles. The distribution of silicon, iron, and copper in the ternary substrate and the overlaying oxide layer is presented in Fig. 18. It is clearly observed that whereas iron and silicon are present at almost similar extend in both the substrate and the oxide layer, copper is significantly reduced in the oxide probably due to the faster outward migration of Cu^{2+} relative to Al^{3+} (ca. 3.2 times, [44]). Residual copper may be observed towards the surface of the oxide (Fig. 18c), in areas where iron and silicon bearing phases are also present, indicating a possible hindering effect by the latter.

4. Conclusions

The effects of substrate cast microstructure on the growth of anodic oxide layers were evaluated by different microscopy techniques (optical microscopy, laser scanning confocal microscopy, and scanning electron microscopy coupled with energy dispersive X-ray spectroscopy).

In the case of pure aluminum substrate, the insoluble impurities (i.e. Al–Fe and Al–Fe–Si particles) were occluded in the oxide layer. A microstructure consisting of uniform grains and a low amount of insoluble impurities is considered necessary to ensure growth of sound anodic oxide layers.

The microstructure of the binary AlSi10 substrate revealed stronger impact on the morphology of the oxide layers, associated with the presence of Si particles and morphology of the aluminum cells. In this case, a fine cell structure and a modified morphology of Si particles are considered favorable for the growth of anodic oxide layers with minimum defects and uniform thickness. Occlusion of Si particles in the oxide layer also affected the morphology of the porous alumina film with development of deflected pores around the particles.

The addition of copper resulted in local changes in layer morphology generated by dissolution of Al_2Cu particles. The effects related to Si particles were preserved.

Acknowledgements

The financial support from the Innovatiegerichte Onderzoekprogramma (IOP) Oppervlaktetechnologie (project IOT 99002), The Netherlands is greatly acknowledged. In addition, thanks are due to Mr. Kees Kwakernaak from the group of Surface and Interface (TUD, The Netherlands) for its help with the SEM/EDS analyses.

References

[1] H. Masuda, K. Nishio, N. Baba, Thin Solid Films 223 (1993) 1.
[2] H. Masuda, K. Fukuda, Science 268 (1995) 1466.
[3] P. Hoyer, K. Nishio, H. Masuda, Thin Solid Films 286 (1996) 88.
[4] O. Jessensky, F. Müller, U. Gösele, Appl. Phys. Lett. 72 (1998) 1173.
[5] A.P. Li, F. Müller, A. Birner, K. Nielsch, U. Göele, J. Appl. Phys. 84 (1998) 6023.
[6] A.T. Shawaqfeh, R.E. Baltus, J. Membr. Sci. 157 (1999) 147.
[7] R.B. Metzger, V.V. Konovalov, M. Sun, T. Xu, G. Zangari, B. Xu, M. Benakli, W.D. Doyle, IEEE Trans. Magn. 36 (2000) 30.
[8] H. Asoh, K. Nishio, M. Nakao, T. Tamamura, H. Masuda, J. Electrochem. Soc. 148 (2001) B152.
[9] G.D. Sulka, S. Stroobants, V. Moshchalkov, G. Borghs, J.-P. Celis, J. Electrochem. Soc. 149 (2002) D97.
[10] W.G. Yelton, K.B. Pfeifer, A.W. Staton, J. Electrochem. Soc. 149 (2002) H1.
[11] S. John, V. Balasubramanian, B.A. Shenoi, Metal. Finish. 82 (1984) 33.
[12] A.D. Juhl, in: Proceedings of the Seventh International Technical Symposium IHAA, San Diego, CA., 10–14 October 1998, p. 1.
[13] H.W. Wang, P. Skeldon, G.E. Thompson, K. Stevens, in: Proceedings of the Second International Symposium, Alum. Surf. Sci. Technol. (ASST 2000), Manchester, U.K., 21–25 May, 2000, p. 588.
[14] M. Sakairi, P. Skeldon, G.E. Thompson, G.C. Wood, K. Stevens, in: Proceedings of the Second International Symposium Alum. Surf. Sci. Technol. (ASST 2000), Manchester, U.K., 21–25 May, 2000, p. 410.
[15] R. Akeret, H. Bichsel, E. Schwall, E. Simon, M. Textor, Trans. Inst. Metal Finish. 68 (1990) 20.
[16] A.K. Mukhopadhyay, V.V. Rama Rao, C.R. Chakravorty, Mater. Sci. Forum 217–222 (1996) 1617.
[17] H. Habazaki, K. Shimizu, P. Skeldon, G.E. Thompson, G.C. Wood, X. Zhou, Trans. Inst. Metal Finish. 75 (1997) 18.
[18] G.E. Thompson, H. Habazaki, K. Shimizu, M. Sakairi, P. Skeldon, X. Zhou, G.C. Wood, Aircr. Eng. Aerosp. Technol. 71 (1999) 228.
[19] L.E. Fratila-Apachitei, J. Duszczyk, L. Katgerman, Surf. Coat. Technol. 157 (2002) 80.
[20] F. Echeverria, P. Skeldon, G.E. Thompson, H. Habazaki, K. Shimizu, J. Electrochem. Soc. 146 (1999) 3711.
[21] J.H.W. de Wit, Electrochim. Acta 46 (2001) 3641.
[22] P. Bailey, P. Skeldon, T.C.Q. Noakes, G.E. Thompson, M. Sakairi, H. Habazaki, K. Shimizu, Surf. Interface Anal. 31 (2001) 480.
[23] C.E. Caicedo-Martinez, G.E. Thompson, E.V. Koroleva, Surf. Eng. 18 (2002) 145.
[24] C.E. Caicedo-Martinez, E.V. Koroleva, G.E. Thompson, P. Skeldon, K. Shimizu, H. Habazaki, G. Hoellrigl, Surf. Interface Anal. 34 (2002) 405.
[25] J.A. Abbott, Adv. Mater. Process 9 (1994) 29.
[26] A.K. Mukhopadhyay, A.K. Sharma, Surf. Coat. Technol. 92 (1997) 212.
[27] J. Sykes, G.E. Thompson, D. Mayo, P. Skeldon, J. Mater. Sci. 32 (1997) 4909.
[28] A.K. Sharma, H. Bhojraj, H. Narayanamurthy, A.V. Patki, Plat. Surf. Finish. 85 (1998) 55.
[29] A.K. Mukhopadhyay, Metall. Mater. Trans. A 29A (1998) 979.
[30] L.E. Fratila-Apachitei, F.D. Tichelaar, J. Duszczyk, L. Katgerman, in: Proceedings of the Fifteenth International Corrosion Congress

(ICC), Granada, Spain, 22–27 September, 2002, CD version paper no. 201.
[31] X. Liu, G. Qi, X. Bian, Mater. Sci. Forum 331–337 (2000) 367.
[32] A.J. Griffin Jr., F.R. Brotzen, J. Electrochem. Soc. 141 (1994) 3473.
[33] G.C. Wood, J.P. O'Sullivan, Electrochim. Acta 15 (1970) 1865.
[34] G.E. Thompson, R.C. Furneaux, G.C. Wood, Trans. Inst. Metal Finish. 55 (1977) 117.
[35] D.R. Gabe, D.H. Ross, A.J. Dowell, in: Proceedings of the second International Symposium Alum. Surf. Sci. Technol. (ASST 2000), Manchester, U.K., 21–25 May, 2000, p. 374.
[36] D.R. Gabe, Trans. Inst. Metal Finish. 78 (2000) 207.
[37] J.R. Davis, Aluminum and Aluminum Alloys, ASM International, Materials Park OH, 1993, p. 32.
[38] T.B. Massalski, J.L. Murray, L.H. Bennett, H. Baker, L. Kacprzak, Binary Alloys Phase Diagram, vol. 1, ASM International, Metals Park OH, 1986, p. 164.
[39] R.N. Caron, J.T. Staley, in: G.E. Dieter (Ed.), Materials Selection and Design vol. 20, ASM Handbook, ASM International, Materials Park OH, 1997, p. 388.
[40] P. Skjerpe, Metall. Trans. A 18A (1987) 189.
[41] A.L. Dons, Z. Metallkde. 76 (1985) 609.
[42] K. Shimizu, G.M. Brown, K. Kobayashi, P. Skeldon, G.E. Thompson, G.C. Wood, Corros. Sci. 40 (1998) 1049.
[43] L.E. Fratila-Apachitei, J. Duszczyk, L. Katgerman, Surf. Coat. Technol. 165 (2003) 309.
[44] H. Habazaki, X. Zhou, K. Shimizu, P. Skeldon, G.E. Thompson, G.C. Wood, Electrochim. Acta 42 (17) (1997) 2627.